

# **Evaluation of Arctic Ocean surface salinities from SMOS against a regional reanalysis and in situ data**

Jiping Xie<sup>1</sup>, Roshin P. Raj<sup>2</sup>, Laurent Bertino<sup>2</sup>, Annette Samuelsen<sup>2</sup>, and  
Tsuyoshi Wakamatsu<sup>2</sup>

1. Nansen Environmental and Remote Sensing Center, N5006 Bergen, Norway
2. Nansen Environmental and Remote Sensing Center and Bjerknes Centre for Climate Research, Bergen, N5006 Bergen, Norway

*Correspondence to:* Jiping. Xie (jiping.xie@nersc.no)

## Abstract

1  
2 Recently two gridded Sea Surface Salinity (SSS) products that cover the Arctic Ocean  
3 have been derived from the European Space Agency's (ESA) Soil Moisture and Ocean  
4 Salinity (SMOS) mission: one developed by the Barcelona Expert Centre (BEC) and  
5 the other developed by the Ocean Salinity Expertise Center of the Centre Aval de  
6 Traitement des Données SMOS at IFREMER (CEC). The uncertainties of these two  
7 SSS products are quantified during the period of 2011-2013 against other SSS  
8 products: one data assimilative regional reanalysis, one data-driven reprocessing in  
9 the framework of the Copernicus Marine Environment Monitoring Services (CMEMS),  
10 two climatologies: the 2013 World Ocean Atlas (WOA) and the Polar science center  
11 Hydrographic Climatology (PHC), and in-situ datasets, both assimilated and  
12 independent. The CMEMS reanalysis comes from the TOPAZ4 system which  
13 assimilates a large set of ocean and sea-ice observations using an Ensemble Kalman  
14 Filter (EnKF). Another CMEMS product is the Multi-OBServations reprocessing (MOB),  
15 a multivariate objective analysis combining in-situ data with satellite SSS. The monthly  
16 root mean squared deviations (RMSD) of both SMOS products, compared to the  
17 TOPAZ4 reanalysis, reach 1.5 psu in the Arctic summer, while in the winter months  
18 the BEC SSS is closer to TOPAZ4 with a deviation of 0.5 psu. The comparison of CEC  
19 satellite SSS against in-situ data shows too fresh Atlantic waters in the Barents Sea,  
20 the Nordic seas, and in the northern North Atlantic Ocean, consistently with the  
21 abnormally fresh deviations against TOPAZ4. When compared against independent  
22 in-situ data in the Beaufort Sea, the BEC product shows the smallest bias (<0.1 psu)  
23 in summer and the smallest RMSD (1.8 psu), although all six SSS products share a  
24 common challenge to represent fresher water masses (<24 psu). Along the Norwegian  
25 coast and at the southwestern coast of Greenland, the BEC SSS shows smaller errors  
26 than TOPAZ4 and indicates the potential value of assimilating the satellite-derived  
27 salinity in this system.

28  
29 **Keywords:** Arctic Ocean; sea surface salinity; SMOS; reanalysis;  
30  
31  
32  
33  
34

## 35        **1. Introduction**

36    The sea surface salinity (SSS) plays a key role in tracking processes in the global  
37    water cycle through precipitation, evaporation, runoff, and sea-ice thermodynamics  
38    (Vialard and Delecluse, 1998; Sumner and Belaine, 2005; Vancoppenolle et al.,  
39    2009; Yu, 2011). SSS is known to impact the oceanic upper mixing significantly (Latif  
40    et al., 2000; de Boyer Montegut et al., 2004; Maes et al., 2006; Furue et al., 2018)  
41    and via its effect on the surface layer density (Johnson et al, 2012). The SSS also  
42    affects the decadal variability of hydrography in the upper waters of the North Atlantic  
43    (Reverdin et al., 1997). Using a coupled atmosphere-ocean model and an observed  
44    SSS climatology dataset, Mignot and Frankignoul (2003) attributed the interannual  
45    variability of the Atlantic SSS to two factors: anomalous Ekman advection and the  
46    freshwater flux. Additionally, the increased melting of glaciers and sea-ice in the  
47    Arctic (McPhee et al., 1998; Macdonald et al., 1999) leads to significant changes in  
48    the salinity distribution and fresh water pathways (Steele and Ermold, 2004; Morison  
49    et al., 2012). The freshwater flux is regarded as one of the least constrained  
50    parameters in ocean models due to poorly known river discharge, precipitation, and  
51    glacial/sea-ice melt (e.g., Tseng et al., 2016; Furue et al., 2018). In ocean models the  
52    sea-surface freshwater flux is often adjusted directly or the SSS is restored to its  
53    corresponding climatological value to avoid salinity drift.

54

55    Monitoring SSS from space is crucial for understanding the global water cycle and  
56    the ocean dynamics, especially in the Arctic Ocean where our knowledge of the SSS  
57    variability is limited due to non-homogenous and sparse in-situ data. The European  
58    Space Agency's (ESA) Soil Moisture and Ocean Salinity (SMOS) satellite, launched  
59    in November 2009, consists of the Microwave Imaging Radiometer using Aperture  
60    Synthesis (MIRAS) instrument, a passive 2-D interferometric radiometer operating in  
61    L-band (1.4 GHz, 21 cm), that measures the brightness temperature (BT) emitted  
62    from the Earth. The L-band microwave is highly sensitive to water salinity, which  
63    influences the dielectric constants in the sea, and is less susceptible to atmospheric  
64    or vegetation-induced attenuation than higher frequency measurements (Font et al.,  
65    2010; Kerr et al., 2010; Mecklenburg et al., 2012). Committed to provide global  
66    salinities averaged over 10-30 days with an accuracy of 0.1 psu in the open ocean,  
67    ESA provides the MIRAS data into SMOS Level 1 (L1) and Level 2 (L2) products  
68    through a set of sequential processors (Mecklenburg et al., 2012; ESA, 2017).

69

70 Over the ocean, Level 2 products (L2OS) are comprised of three different ocean  
71 salinities, together with the BTs at the top of atmosphere and at the sea surface,  
72 distributed by ESA with swath-based format (e.g., SMOS Team, 2016; ESA, 2017).  
73 As a result of the efforts of the national agencies in France and Spain respectively,  
74 two Level 3 (L3) data products of SSS are freely available, which are independently  
75 developed by the Ocean Salinity Expertise Center (CECOS) of the Centre Aval de  
76 Traitement des Données SMOS at IFREMER and the Barcelona Expert Centre.  
77 These two SMOS products have successfully resolved the Agulhas salinity front  
78 (D'Addezio et al., 2016) and proven useful for the estimating precipitation (Supply et  
79 al., 2018). The work of Olmedo et al. (2018) quantitatively evaluate the accuracy of  
80 the SMOS Arctic and sub-Arctic SSS to less than 0.35 psu, but this evaluation  
81 against Argo data was limited by the lack of data in the Arctic proper. The present  
82 study thus investigates the accuracy of these two SMOS SSS products in the Arctic  
83 Ocean.

84

85 A good estimate of surface salinity is a necessary step towards the knowledge of the  
86 three-dimensional water mass properties, for which data assimilation and optimal  
87 interpolation methods must be invoked. In a recent study, Uotila et al. (2018)  
88 investigated the Arctic salinity in ten reanalysis products and found disagreements  
89 within them regarding the seasonal cycle in the upper layer (0-100 m; Figure 12 of  
90 Uotila et al., 2018). Note that the full assessment of the Arctic SSS products has  
91 been hindered by the extreme paucity of in-situ data in the Arctic. The SSS data from  
92 the SMOS mission should in principle allow the evaluation of salinity on a basin  
93 scale. In this study, we use two SSS products available from the Copernicus Marine  
94 Environment Monitoring Service (CMEMS). The first is the regional Arctic CMEMS  
95 reanalysis (ARCTIC-REANALYSIS-PHYS-002-003) from the TOPAZ4 assimilation  
96 system, which is a coupled ocean and sea-ice data assimilation system using the  
97 Ensemble Kalman filter (EnKF) to assimilate the various ocean and sea-ice  
98 observations (e.g., Xie et al., 2017). The second is the CMEMS multivariate optimal  
99 interpolation reprocessing (MULTIOBS\_GLO\_PHY\_REP\_015\_002, Droghei et al.,  
100 2018). The latter product directly merges in-situ data with satellite measurements  
101 including SMOS without the use of a model and is therefore a reprocessing rather  
102 than a reanalysis. There are four other global reanalysis products under CMEMS,

103 but understanding well their differences requires an intimate knowledge of their  
104 setup, and is out of scope of the present study.

105

106 We assess the quantitative deviations of Arctic SSS among the two SMOS products  
107 and the two CMEMS products, together with two climatology datasets: WOA13  
108 (version 2.0 of World Ocean Atlas of 2013; Zweng et al., 2013) and the older PHC  
109 (Polar Science Center Hydrographic Climatology version 3.0; Steele et al., 2001). We  
110 further extend the evaluation using available in-situ salinity observations during the  
111 years 2011-2013 from different data sources. Can the evaluation against the in-situ  
112 data also shed light on the uncertainty of the SMOS products? Can it also give useful  
113 information needed for the assimilation of the SMOS SSS products into an Arctic  
114 ocean forecast/reanalysis system?

115

116 The paper is organized as follows: Section 2 describes all SSS products and the in-  
117 situ datasets. The monthly mean SSS from these six products are intercompared and  
118 monthly differences from the TOPAZ SSS are analyzed in Section 3. Section 4  
119 evaluates the SSS products against in-situ data, which are divided between  
120 assimilated and independent data. A summary of this study is provided in Section 5.

121

## 122 **2. Data description**

### 123 *2.1 Sea surface salinity from SMOS*

124 The SSS retrieval from SMOS is subject to biases originating from various non-  
125 geophysical sources such as the so-called land-sea contamination and the latitudinal  
126 biases, mainly caused by the thermal drift of the instrument. A particular challenge in  
127 the Arctic is the sea-ice edge because of ice-ocean contamination. Based on  
128 different statistical approaches, match-up criteria, and SMOS data filtering flags, two  
129 centers have developed separate processing chains producing a Level 3 SSS  
130 product on a regular grid. These two SSS products are hereafter named respectively  
131 CEC and BEC in this study, evaluated during the three years of 2011-2013 (see  
132 Table 1).

- 133 • *The BEC product*

134 The latest regional Arctic product (version 2.0) from BEC is available from  
135 <http://bec.icm.csie.es> since December 2018 (last access: March 2019). The BEC  
136 SSS product was generated from ESA L1B (v620) products, and accumulates salinity

137 data over 9 days with a spatial grid resolution of 25 km. With respect to its previous  
138 version, a systematic bias in the retrieved salinity is corrected by computing the  
139 SMOS climatology (the most probable value for a given lat-lon, incidence angle and  
140 across-swath distance) which is substituted by a reference value from WOA13. In  
141 addition, a temporal bias correction has been refined in this version using near-  
142 surface Argo salinity to compute regional averages (see the details in Olmedo et al.,  
143 2018).

144       • *The CEC product*

145 The third version of LOCEAN SMOS SSS L3 maps (L3\_DEBIAS\_LOCEAN\_v3) was  
146 released by the CECOS in July 2018. Every 4 days, the SSS maps averaged over 9  
147 days are released on <ftp.ifremer.fr> (last access: December 2018). This product uses  
148 the Equal-Area Scalable Earth Grid (EASE-Grid) which has limited grid distortion and  
149 a spatial resolution of 25km. Using a Bayesian retrieval approach (Kolodziejczyk et  
150 al., 2016), the SMOS systematic errors in the vicinity of continents are discarded to  
151 improve the product quality. Further, a ‘de-biasing’ method (Boutin et al., 2018) has  
152 been applied in this version of the CEC product, in which the non-Gaussian  
153 distribution of SSS is taken into account, refining the latitudinal correction at high  
154 latitude, and preserving the naturally seasonal variability of SSS.

155

156       2.2 *Sea surface salinity from two CMEMS products*

157       • *The TOPAZ4 Arctic MFC reanalysis*

158 TOPAZ4 uses the version 2.2 of Hybrid Coordinate Ocean Model (HYCOM,  
159 Chassignet et al., 2003; Bertino and Lisæter, 2008) coupled with a simple  
160 thermodynamic sea ice model (Drange and Simonsen, 1996) in which the elastic-  
161 viscous-plastic rheology describes the sea ice dynamics (Hunke and Dukowicz,  
162 1997). The model domain covers the Arctic Ocean and the north Atlantic Ocean with  
163 a horizontal resolution of 12-16 km. In order to obtain an accurate and dynamically  
164 consistent reanalysis in the Arctic Ocean, the deterministic EnKF (DEnKF; Sakov and  
165 Oke, 2008) was implemented in TOPAZ with a dynamical ensemble of 100 members  
166 all driven by perturbed 6-hourly atmosphere forcing from ERA interim (Simmons et  
167 al., 2007). The perturbations of precipitations are following a log-normal probability  
168 distribution and conserve the ensemble-average total precipitation.

169 Along the model lateral boundaries in the South Atlantic and in Bering Strait, the  
170 temperature and salinity are relaxed to a combined climatology data from PHC and

171 WOA. The river discharges are treated as an additional mass and a negative salinity  
172 flux. Near the surface, to avoid the salinity drift (Tseng et al., 2016; Furue et al.,  
173 2018), a weak relaxation to the same combined climatological SSS with 30 days  
174 decay is used as most ocean models, but restricted to the areas where the difference  
175 to climatology is smaller than 0.5 psu. The EnKF assimilates various ocean and sea-  
176 ice observations (e.g., Xie et al., 2016, 2018) into a multivariate state update of the  
177 HYCOM model.

178 The understanding for the uncertainty of the TOPAZ4 SSS has been hindered by  
179 poor coverage of in-situ data over the Arctic domain, although Xie et al. (2017) had  
180 comprehensively assessed the TOPAZ4 reanalysis during 1991-2013 against various  
181 types of ocean and sea-ice observations. For the sake of brevity, the TOPAZ4  
182 reanalysis SSS is named TP4 hereafter.

183

184 • *SSS from the Multi-Observations dataset*

185 The CMEMS product of MULTIOBS\_GLO\_PHY\_REP\_015\_002 combines the SSS  
186 observations from in-situ and satellite data, using optimal interpolation (OI,  
187 Buongiorno Nardelli et al., 2016; Verbrugge et al., 2018) at weekly interval on a 0.25°  
188 x 0.25° regular grid. The main datasets used during the OI processing are: 1) the  
189 quality controlled in-situ data, COriolis dataset for Re-Analysis (CORA, Cabanes et  
190 al., 2013) distributed through CMEMS; 2) the objectively analyzed SSS and SST data  
191 generated from CORA, also distributed by CMEMS, which uses the WOA 2013  
192 climatology as first guess and has been upscaled to the MOB grid as another first  
193 guess of the multidimensional OI; 3) The SMOS L3 binned (L3bin) data reprocessed  
194 by SMOS-BEC at 0.25° grid, although the previous version 1.0 of the product  
195 mentioned above; 4) The daily Reynolds L4 AVHRR\_OI Global blended SST product  
196 on a 0.25° grid. This product is called MOB hereafter.

197

198 *2.3 Surface salinity from in-situ data*

199 The in-situ SSS data are acquired here from three quality-controlled datasets. The  
200 first data source is CORA from CMEMS (product id:  
201 INSITU\_GLO\_TS\_REP\_OBSERVATIONS\_013\_001\_b), also used in the MOB SSS.  
202 CORA contains temperature and salinity profiles from various in-situ data sources  
203 (Cabanes et al., 2013). Since 2013, the CORA dataset has been updated every year

204 and includes all the Argo float profiles, moorings, gliders, Ice-Tethered Profilers (ITP;  
 205 Toole et al., 2011), XBT, CTD, and XCTD data. The latest version of the dataset,  
 206 CORA5.1, covers the period of 1950-2016. Figure 1a shows the distribution of SSS  
 207 (averaged over 0-8 m depth) observations from CORA5.1 (total 69,246 observations)  
 208 over the domain north of 52°N during the years 2011-2013.

209 The second source of in-situ data is from the Beaufort Gyre Experiment Project  
 210 (BGEP, <http://www.whoi.edu/website/beaufortgyre/background>, last access: 14<sup>th</sup>  
 211 December 2018). In order to monitor the natural variabilities of the Beaufort Sea in  
 212 the Canada Basin, BGEP maintains moorings since 2003 and acquires in-situ  
 213 measurements over the Beaufort Sea region every summer. Symbols (anti-triangle,  
 214 square, and star) shown in Fig. 1b indicate the locations of valid SSS observations  
 215 obtained from BGEP. The in-situ dataset used in this study is obtained from the GO-  
 216 SHIP (the Global Ocean Ship-based Hydrographic Investigations Program, Talley et  
 217 al., 2017) database under the Climate Variability and Predictability Experiment  
 218 (CLIVAR). The SSS observations in the Beaufort Sea are extracted from  
 219 CLIVAR/GO-SHIP data with EXPOCODE (33HQ20111003 and 33HQ20121005, ref.  
 220 Mathis and Monacci, 2014), which are available from [https://cdiac.ess-  
 221 dive.lbl.gov/ftp/oceans/CARINA/Healy/](https://cdiac.ess-) (last access: 18th December 2018). All the  
 222 valid salinity profiles are averaged within the upper 8 m layer, in order to match at  
 223 best with the satellite SSS measurements. Contrarily to the CORA data, both BGEP  
 224 and CLIVAR data are independent from all the evaluated datasets.

225

### 226 **3. Intercomparison of monthly SSS fields**

227 Prior to the intercomparison of different SSS products, all the gridded products from  
 228 satellite, reanalysis and climatology have been mapped on the same grid used in the  
 229 TP4 model by a “nearest neighbor” interpolation. To quantitatively evaluate the SSS  
 230 deviation in the Arctic, the bias and the root mean square deviation (RMSD) are  
 231 defined by

$$232 \quad \text{Bias} = \frac{1}{p} \sum_{i=1}^p (\mathbf{H}_i \mathbf{x}_i^f - \mathbf{s}_i) \quad (1)$$

$$233 \quad \text{RMSD} = \sqrt{\frac{1}{p} \sum_{i=1}^p (\mathbf{H}_i \mathbf{x}_i^f - \mathbf{s}_i)^2} \quad (2)$$

234 Where  $p$  is the length of the time series,  $\mathbf{x}_i^f$  is the valid salinity from different sources  
235 at the  $i$ th time, compared to the reference salinity field  $\mathbf{s}_i$ .  $\mathbf{H}_i$  is the observation  
236 operator projecting  $\mathbf{x}_i^f$  onto  $\mathbf{s}_i$ .

237

238 • *Monthly mean comparison of SSS*

239 Figure 2 shows the monthly mean Arctic SSS in March from the six products. Notable  
240 differences in the two SMOS products appear in the Nordic Seas, Barents Sea, and  
241 around the Labrador Sea in the northern North Atlantic Ocean. At first sight, the  
242 large-scale SSS features from SMOS products are similar to the other products.  
243 However, the CEC SSS is fresher (as shown by the isolines of 35 psu) compared to  
244 the BEC, TP4, MOB and both climatologies. The location of the sea-ice edge in the  
245 two SMOS products match comparatively well with the TP4 reanalysis (Fig. 2a, d). In  
246 sea-ice covered region, TP4 shows a gradual decrease in SSS from the European to  
247 the American sector, with two minima near the Beaufort Sea and the East Siberian  
248 Sea (ESS; Fig. 2b) consistently with the PHC (Fig. 2c). Those are unclear in the  
249 MOB and WOA (Fig. 2e, f), especially the SSS minimum in the Beaufort Sea. The  
250 latter two products also show artificial projection artefacts around the North Pole.  
251 Figure 3 shows the corresponding SSS fields in September. In comparison to the  
252 March situation, the BEC and CEC SSS in the Nordic Seas are both less saline,  
253 indicated by the 35 psu isoline. The sea ice masking of the two SMOS products differ  
254 considerably in the Canadian Basin and in the Arctic marginal seas. Although the  
255 SSS of TP4, MOB, PHC and WOA agree relatively well in the northern Atlantic  
256 Ocean, the discrepancies become dramatic in ice-covered areas. Below the ice or  
257 near the sea-ice edge (denoted by the brown thick line in Fig. 2 and 3), TP4 and PHC  
258 share common features, which can be explained by the model restoring to PHC. On  
259 the other hand, the MOB and WOA differ significantly in spite of WOA being used as  
260 input to the MOB. Short of a universal reference for Arctic SSS, the monthly mean  
261 SSS deviations will be quantified using TP4 as a reference.

262

263 • *Deviation analysis of monthly SSS referred to TP4*

264 Figure 4 and Figure 5 show the deviations of the monthly mean SSS of the five  
265 products with reference to the TP4 SSS in August and September respectively. In  
266 August, the two SMOS products (Fig. 4a, c) show coherently negative deviations (~2

267 psu) in the marginal seas of the Beaufort Sea, the ESS, the Laptev Sea, and the  
268 Kara Sea. In the North Atlantic Ocean, away from the sea-ice edge, the deviation of  
269 the BEC from TP4 is lower (bias less than 0.5 psu). Focusing on the Arctic domain  
270 ( $>60^{\circ}\text{N}$ ), the mean deviation of the BEC SSS is -0.87 psu and its root mean square is  
271 1.75 psu. The CEC SSS shows considerable negative deviations over 1 psu in the  
272 northern Atlantic, from north of Denmark Strait to the west coast of Ireland. This is  
273 remarkably different from the BEC, and does not discern the subpolar from the  
274 subtropical waters there (Hátún et al., 2005). The deviations of MOB and the two  
275 climatology products are comparatively small in the open ocean of the northern  
276 Atlantic (Fig. 4b, e). Near and below the sea-ice cover, the deviations are much  
277 larger, particularly both the MOB and WOA show strong saline anomalies ( $> 1$  psu) in  
278 the Eurasian basin and low anomalies in the American basin.

279

280 In September, the SSS deviations of BEC, MOB, PHC and WOA show similar fresher  
281 patterns as in August, but the CEC deviations becomes surprisingly positive around  
282 the ice edge. The SSS deviation of CEC, averaged over the Arctic domain ( $>60^{\circ}\text{N}$ ),  
283 swaps from -0.42 to 0.42 psu from one month to the next one. The seasonal  
284 evolution of monthly SSS deviations from TP4 for all five remaining products,  
285 averaged over the Arctic, are shown in Fig. 6. Among the five products, the MOB  
286 shows the strongest seasonality with the RMSD higher than 4 psu in July and August  
287 (Fig. 6a), and close to 2 psu in winter. The spatially averaged deviation is much  
288 fresher than TP4, over -2 psu in summer and -0.5 psu in winter (Fig. 6b). The  
289 deviations of the two SMOS SSS show a relatively smaller seasonality (Fig. 6a).  
290 During summer months, their RMSDs reach 1.5 psu (Fig. 6a) in summer, and they  
291 decrease to 0.5 and 1.0 psu (for BEC and CEC respectively). Throughout the whole  
292 year, the BEC RMSDs (Fig. 6a) are consistently smaller than that of CEC, and the  
293 seasonal cycles are different. This shows that the BEC SSS is closest to TP4,  
294 although it is overall fresher in the Summer.

295

#### 296 **4. Evaluation against in-situ observations**

297 The misfits of the six SSS products from SMOS, CMEMS and climatologies are  
298 calculated as in Eqs. (1) and (2) against the pointwise in-situ observations described  
299 in Section 2.3. For TP4, the SSS evaluation is conducted on the same model day as

300 the in-situ observations. Owing to the fact that the SSS from BEC, CEC and MOB are  
301 averaged over either 9 days or one week (see Table 1), the product dates at the  
302 center of the averaging window lag 5 or 4 days compared to the observation date.  
303 For PHC and WOA, the in-situ observations are sorted to monthly bins and evaluated  
304 for each month. The quantitative evaluation is divided into two main sections starting  
305 with dependent and then independent observations.

306

#### 307 *4.1 Against SSS from CORA5.1*

308 As shown in Fig. 1a, the distribution of SSS observations from CORA5.1 over the  
309 Arctic is very inhomogeneous during the three years. Due to this, the evaluation of  
310 the gridded SSS products against in-situ observations is restricted to the observation-  
311 rich regions. The SSS misfits bias and RMSD for the six products are reported in  
312 Table 2 according to the eight Arctic sub-regions defined previously (Figure 1a). The  
313 observations are displayed on scatterplots (Figure 7 and 8) to exhibit their  
314 uncertainties for fresh and saline waters in different areas.

- 315 • *Central Arctic*

316 Figure 7 shows the SSS products compared with discrete observations in the central  
317 Arctic (sub-regions S0, S1, S2, and S3). The observed SSS in S0 and S1 are mainly  
318 from the ITP at a minimal depth of 8 m. Around the North Pole (S0), where the  
319 satellite SSS are absent, the TP4 reanalysis and MOB reprocessing show opposite  
320 biases: +0.48 psu and -0.52 psu respectively (Table 2). The two climatologies used  
321 by them, PHC and WOA respectively, also show opposite biases. Considering the  
322 latter climatologies, both SSS scatterplots shows a fresh bias for high salinity water  
323 (>33 psu) and a saline bias for low salinity water (<31 psu).

324 In the Canadian basin (in S1), the two climatological SSSs show an obvious gap in  
325 comparison to the ITP observations. Comparing to the fresh in-situ SSS from 24 to  
326 30 psu, the PHC has strong saline bias (from 2 to more than 5 psu). On the other  
327 hand, the WOA shows both a fresh bias for relatively high salinity water (>28 psu)  
328 and saline bias for fresher water (<26 psu). Owing to the different time periods (Table  
329 1) of the in-situ data they used, this result confirms the freshening of the Canadian  
330 basin since in the 1990s (Morison et al., 2012).

331 In the S1 sub-region, the satellite SSS from BEC and CEC have only 20 and 42 data  
332 points for evaluation respectively. The resulting scatterplots show a significantly

333 positive salinity bias ( $>4$  psu) for fresh waters ( $<27$  psu). For relatively higher salinity  
334 water ( $> 27$  psu), the CEC has a stronger saline bias than the BEC.

335 In the Kara Sea (sub-region S2), the TP4 SSS has the smallest RMSD at 1.7 psu,  
336 which is significantly smaller than other products. The scatterplot also shows a good  
337 linear relationship between the TP4 and the in-situ SSS, while other products  
338 generally show fresh biases, indicating that the SSS variability in the Kara Sea is well  
339 captured by TP4. In the Barents Sea (sub-region S3), TP4 gives as well the smallest  
340 misfit (RMSD: 0.34 psu; bias: -0.14 psu). The SSS scatterplots exhibits linear  
341 relationships for all products except the CEC, which underestimates the Atlantic  
342 water SSS.

343

344 • *Northern North Atlantic and Nordic Seas*

345 Figure 8 shows the paired scatterplots of the six SSS products in the subpolar seas  
346 from sub-regions S4 to S7 (see Fig. 1a). In S4 and S5, the bias of SSS products is  
347 relatively small, less than 0.15 psu (Table 2), except for CEC in S4 and TP4 in S5,  
348 both too saline by 0.2 psu. The scatterplots further indicate that low salinity waters  
349 are too saline in all SSS products in S4 ( $<31$  psu) and in S5 ( $<28$  psu). Meanwhile,  
350 the respective bias and RMSD of the SSS products are less than 0.1 psu and 0.43  
351 psu respectively, except for the CEC in S6 and S7. The MOB SSS has the smallest  
352 salinity bias. Among the eight regions compared here (S0 to S7), the SSS bias is  
353 lowest in S6 (Irminger Sea).

354 Over the northern North Atlantic and the Nordic seas, Fig. 9 shows maps of the mean  
355 SSS deviation for each product during the period 2011-2013. Considerable negative  
356 biases ( $<-0.2$  psu) are found in the CEC, whereas the MOB and WOA have the  
357 smallest bias, less than 0.02 psu (Fig. 9 d, e, f). The SSS products from BEC, TP4  
358 and PHC (Fig. 9 a, b, c) have slightly higher bias ( $\sim 0.05$  psu) in comparison to the  
359 MOB and WOA. On average, the BEC bias is only -0.04 psu, much smaller than that  
360 of the CEC ( $<-0.2$  psu). Focusing on the BEC SSS, Fig 9a shows that while a fresh  
361 bias dominates the Nordic Seas, the product is too saline in the northern North  
362 Atlantic and the North Sea.

363 The inter-comparison of the biases against the in-situ data in Fig. 9a and 9b exhibits  
364 two strong positive biases of TP4 along the Norwegian coast and along the West  
365 Greenland coast. Notably, the BEC has smaller bias along both coasts, although it  
366 has a slightly saline bias offshore. This indicates potential benefits of the BEC SSS

367 for the TOPAZ system along the Norwegian and Greenland coasts, were it  
368 successfully assimilated into the system. Figure 10 shows RMSDs of SSS for all the  
369 products over the northern North Atlantic Ocean and the Nordic Seas. On average,  
370 the largest uncertainty is found with the CEC (~1.0 psu; Fig. 10d), with RMSDs as  
371 large as 1.5 psu in the Greenland Sea and the Barents Sea. The SSS RMSDs for the  
372 five other SSS products are much smaller (~0.5 psu).

373

#### 374 *4.2 Independent SSS in the Beaufort Sea*

375 Independent in-situ data from BGEP and CLIVAR are used during the summer  
376 months of 2011-2013 in the Beaufort Sea for the evaluation of the six SSS products  
377 (Fig. 11). The in-situ SSS observations range from 15 to 32 psu. The range of BEC  
378 SSS is limited to 24 to 31 psu with a minor bias of 0.09 psu and a RMSD of 1.82 psu.  
379 On the other hand, the range of TP4 SSS is even shorter from 19 to 32 psu, with a  
380 large saline bias of 2.59 psu and a RMSD of 3.63 psu. The linear regression  
381 coefficients for BEC and TP4 are 0.57 and 0.07 respectively. Looking at the low-  
382 salinity observations (~27 psu) collected at (136.4°W, 70.5°N) on 15<sup>th</sup> August 2011,  
383 marked by anti-triangles (Fig. 1b) near the Mackenzie River estuary, TP4 has a  
384 significant negative bias (< -4 psu) visible as the outliers above the dashed-black line  
385 in Fig. 11a. This hints to a lack of fresh water signatures from river discharge.  
386 The range of PHC SSS climatology is only reaching from 24 to 31 psu, similar to  
387 TP4, with a saline bias of 1.65 psu and RMSD of 2.85 psu. Compared to the TP4  
388 deviation at the Mackenzie River basin, the PHC saline bias is present, but smaller.  
389 The strong positive bias in TP4 at these points can then be partly attributed to the  
390 SSS relaxation of the TOPAZ model towards the PHC climatology, albeit rather  
391 weak. The range of the WOA is much wider, from 12 to 31 psu. Among the six  
392 products, the WOA bias is the smallest (~0.02 psu) over the Beaufort Sea during all  
393 three summers. However, it should be noted that the variability of in-situ observations  
394 is very large for salinities lower than 24 psu, which contributes to the large RMSD  
395 (>3.0 psu) of both PHC and WOA. It confirms that the two climatologies have a  
396 sizable uncertainty over low salinity regions (<24 psu) in the Arctic Ocean.  
397 The CEC SSS ranges from 13 psu to 34 psu, which is much wider than the range of  
398 the BEC SSS. The saline bias of CEC is however larger at 2.38 psu and its RMSD is  
399 about quite large at 3.77 psu. Furthermore, the CEC deviations from the in-situ  
400 observations are larger in waters fresher than 27 psu. The MOB combined product

401 performs poorly with the largest negative bias (>5 psu) and an RMSD in excess of 8  
402 psu. In contrast to the other five SSS products, the anomalously fresh SSS observed  
403 around the point (140°W, 71°N) near the Mackenzie River estuary are represented  
404 by even fresher values of 12 psu in MOB, which may hint at an amplification of the  
405 anomalies.

406 In order to characterize dependencies of the bias for the six SSS products against  
407 the in-situ data, their absolute differences are plotted as a function of observed SSS  
408 in Fig. 12. In general, all products show considerable deviations with the maxima  
409 reaching 8 to 14 psu. While the absolute misfits of most of the SSS products  
410 monotonically increase towards lower salinity, the bias of MOB shows its peak  
411 around 20 psu shown in Fig. 12c. The fourth-order polynomial curve function,

$$F(S) = p_1S^4 + p_2S^3 + p_3S^2 + p_4S + p_5 \quad (3)$$

412 is then fitted to the absolute bias for each of the SSS products, where S represents  
413 the in-situ salinity. The fitting coefficients,  $p_1$  to  $p_5$ , for each product are listed in Table  
414 3. The norm residuals are displayed on each panel in Fig. 12 and clearly show that  
415 fitting for MOB has the largest uncertainty, while the minimal norm residuals are  
416 about 10 and 7 psu<sup>2</sup> respectively for BEC and TP4. This suggests the derived fitting  
417 curves for BEC and TP4 have credible skill in characterizing its error distribution as a  
418 function of the observed SSS. Both curves monotonically decrease towards the  
419 salinity higher than 28 (30) psu for BEC (TP4) and increase slightly afterwards. The  
420 absolute bias in TP4 is consistently larger than that in BEC. The fitted curves of PHC  
421 and WOA have the similar functional forms to TP4 and BEC, but with lower  
422 amplitudes.  
423

424

## 425 5. Conclusions

426 To understand the uncertainties in the Arctic SSS, our study evaluates the two  
427 gridded SMOS SSS products (BEC and CEC), two CMEMS products (TP4 and  
428 MOB), and two climatology products (PHC and WOA) by their inter-comparison and  
429 comparisons against both of dependent and independent in-situ datasets during the  
430 years of 2011-2013.

431 The differences in the spatial coverage of the two SMOS SSS were clearly shown in  
432 the monthly mean (Fig. 2 and Fig.3), due to the different retrieval applied in these two  
433 datasets. The spatial distributions of SSS from TP4 and PHC are considerably close  
434 to each other, mainly as for the fact that the SSS in the TOPAZ model is relaxed

435 towards PHC at each time step. Relative to TP4, the SSS deviations of the four  
436 products (BEC, MOB, WOA and PHC) in summer show similar magnitude over the  
437 open waters. On the contrary, the CEC SSS shows a negative bias ( $<-1$  psu) over  
438 the region extending from the Iceland towards the western side of Ireland (Fig. 4, 5),  
439 but clearly the BEC SSS has a slightly negative bias over the region. In general, the  
440 most significant differences in the SSS deviations relative to TP4 are found under the  
441 sea-ice cover and in its surrounding marginal ice zones.

442 Furthermore, the intercomparison of the SSS products shows that the BEC SSS in  
443 August and September (Fig. 4, 5) has consistent negative deviations along the sea-  
444 ice edge in the Beaufort Sea and the Chukchi Sea, but the CEC SSS has opposite  
445 deviations in these two months. Thus, it may be arguable that the two SMOS  
446 products would give rise to significantly different effects to the upper ocean state in  
447 the TOPAZ system if it to be assimilated into. Hence the SSS quantitative  
448 evaluations of two products for optimal selection or blending would be worth of  
449 investigating further.

450 Focusing on the wide Arctic domain ( $>60^{\circ}\text{N}$ ), the deviations of the five SSS products  
451 relative to TP4 show diverse seasonal characteristics (Fig. 6). Although the SSS  
452 products of BEC and CEC have the similar deviation of about 1.5 psu (Fig. 6a) in  
453 summer, the BEC deviations in winter months are clearly lower ( $\sim 0.5$  psu). The  
454 deviations of MOB and WOA (Fig. 6a) varies from over 1.5 psu in winter to around 4  
455 psu in summer, which suggests a considerable gap with the TP4. Consequently, the  
456 intercomparison suggests that the BEC SSS has the most consistent pattern with the  
457 TP4 SSS among all other SSS products.

458 Against the in-situ data from CORA5.1 which were used in both TP4 and MOB, the  
459 quantitative evaluations of the six SSS products were investigated in the eight sub-  
460 regions (Fig. 1a). It was divided into two parts: in the central Arctic Ocean; the  
461 northern North Atlantic Ocean and the Nordic Seas. Due to the limited coverage of  
462 BEC and CEC in S1, the scatterplots (Fig. 7) show a positive saline bias ( $>4$  psu) for  
463 low salinity water ( $< 27$  psu). However, the salinity bias of BEC is slightly reduced for  
464 relative high salinity water ( $> 27$  psu). In the Kara Sea and the Barents Sea, the TP4  
465 SSS has the minimal RMSD compared with others (Table 2). The BEC scatterplots in  
466 S2 and S3 (Fig. 7) have similar distributions with respect to TP4.

467 In the northern North Atlantic Ocean and the Nordic Seas (S6, S4, and S3; Fig. 8),  
468 the scatterplots of the CEC SSS show that it underestimates the Atlantic water

469 salinity, which also is consistent with the intercomparison results (low salinity  
470 deviation) shown in Fig. 4 and 5. The misfits of mean and RMSDs shown in Fig. 9  
471 and 10, suggest the CEC SSS has considerable uncertainty (RMSD of about 1 psu),  
472 especially in the Nordic Seas with obvious low salinity biases. On the other hand, the  
473 SSS uncertainties of the BEC are significantly lower in comparison to the CEC, but  
474 are equivalent compared with TP4 and PHC. Two notable regions where the BEC  
475 SSS has lower uncertainties referred to the in-situ observations than the TP4 are  
476 along the Norwegian coast and near the west coast of Greenland Island. It is  
477 reasonable to expect that they are the most beneficial region in the Nordic Seas if the  
478 BEC SSS is successfully assimilated into the TOPAZ system.

479 Against independent in-situ observations from BGEP and CLIVAR, the SSS  
480 evaluation in the Beaufort Sea is performed in the summers of the three years.  
481 The linear regression against these independent SSS observations (Fig. 11)  
482 suggests the BEC SSS has the smallest RMSD of 1.8 psu with a positive bias of 0.1  
483 psu, and the CEC SSS has larger RMSD of about 3.8 psu with a larger positive bias  
484 of 2.4 psu (Fig. 11). On the other hand, the TP4 SSS also shows large RMSD of  
485 about 3.6 psu with large positive bias of 2.6 psu. They are smaller than MOB which  
486 has the RMSD of 8.2 psu and larger negative bias (-5.0 psu). As for the two  
487 climatology products, the RMSDs of WOA and PHC both are more than 2.8 psu, but  
488 with significantly smaller bias in WOA. Overall, the large uncertainty found in the  
489 linear regression of all products is attributed to large product-observation mismatch  
490 against in-situ salinity data of less than 24 psu, which are observed over the  
491 continental shelf near the estuary of the Mackenzie River.

492 In order to characterize the product-data misfits of all six products against in-situ  
493 data, a 4th order polynomial function is fitted to the absolute deviation as a function  
494 of observed salinity (Fig.12). The absolute deviations of most of the products except  
495 for MOB monotonically decrease as observed salinity increases. The norm residuals  
496 for TP4 and BEC and are the smallest of 10.2 and 7.0, respectively, among all six  
497 products and the fitted curves give certain confidence in estimating the size of the  
498 error in the each SSS product. The fitted curve reaches its smallest value of less than  
499 1.0 psu at the in-situ salinity of 28 psu and 30 psu for BEC and TP4 respectively.  
500 Both the fitted curves for CEC and MOB have large norm residuals of 18.1 and 68.8  
501 psu<sup>2</sup> respectively. Note that special attention must be paid in usage of MOB in the

502 Arctic Ocean due to its large negative bias and the RMSD in regions where the  
503 product is based on limited number of observations.  
504 Evaluations of the SSS products against TP4 product and in situ data conducted  
505 above suggest certain benefit can be expected in assimilating one of the SMOS  
506 salinity products, the BEC SSS, into the TOPAZ Arctic ocean analysis-forecast  
507 system. The knowledge of error structure in the SSS products provided in this study  
508 will assist to reasonably estimate the observation error for the SMOS product, which  
509 is required by a data assimilation system. We recommend that due to the poor spatial  
510 coverages of CORA in situ data in the Arctic Ocean, more data - especially from the  
511 Arctic Ocean marginal seas - should be compiled from independent data source for  
512 validating the SMOS SSS products. In addition, when comparing the two climatology  
513 products, PHC and WOA, the SSS scatterplots of the PHC in the central Arctic (Fig.  
514 7) show salinity bias for low saline water. Considering the different time periods of  
515 their compiled in-situ data sources (Table 1), it independently verifies that the  
516 freshening in the Canada Basin since 1990s is rather significant as discussed by  
517 Morison et al. (2012). Based on this evaluation, the next TOPAZ system will use the  
518 WOA to replace the PHC as the target relaxation field.

519

## 520 **Acknowledgement**

521 The authors acknowledge the support of CMEMS for the Arctic MFC and partly  
522 funding from the European Space Agency in response to the Arctic+Salinity project  
523 (Dec 2018-June 2020). Grants of computing time (nn2993k and nn9481k) and  
524 storage (ns2993k) from the Norwegian Sigma2 infrastructures are gratefully  
525 acknowledged. The BEC SSS is produced by the Barcelona Expert Centre  
526 (bec.icm.csic.es) mainly funded by the Spanish National Program on Space. The  
527 CEC SSS is distributed by the Ocean Salinity Expertise Center (CECOS) of CATDS  
528 at IFREMER, France.

529

## 530 **Reference:**

531 Bertino, L., and Lisæter, K. A.: The TOPAZ monitoring and prediction system for the Atlantic  
532 and Arctic Oceans, *Journal of Operational Oceanography*, 1(2), 15–19, doi:  
533 10.1080/1755876X.2008.11020098, 2008  
534 Boutin J., Vergely J.L., Marchand S., D'Amico F., Hasson A., Kolodziejczyk Nicolas, Reul  
535 Nicolas, Reverdin G., Vialard J.: New SMOS Sea Surface Salinity with reduced systematic

536 errors and improved variability. *Remote Sensing of Environment*, 214, 115-134,  
537 <http://doi.org/10.1016/j.rse.2018.05.022>, 2018.

538 Buongiorno Nardelli, B., Droghei, R., and Santoleri, R.: Multi-dimensional interpolation of  
539 SMOS sea surface salinity with surface temperature and *in situ* salinity data. *Remote*  
540 *Sens. Environ.* 180, 392–402. doi: 10.1016/j.rse.2015.12.052, 2016

541 Cabanes, C., A. Grouazel, K. von Schuckmann, M. Hamon, V. Turpin, C. Coatanoan, F. Paris,  
542 S. Guinehut, C. Boone, N. Ferry, C. de Boyer Montégut, T. Carval, G. Reverdin, S.  
543 Pouliquen, and P. Y. Le Traon: The CORA dataset: validation and diagnostics of in-situ  
544 ocean temperature and salinity measurements. *Ocean Science*, 9, 1-  
545 18, <http://www.ocean-sci.net/9/1/2013/os-9-1-2013.html>, doi:10.5194/os-9-1-2013, 2013

546 Chassignet, E. P., Smith, L. T., and Halliwell, G. R.: North Atlantic Simulations with the Hybrid  
547 Coordinate Ocean Model (HYCOM): Impact of the vertical coordinate choice, reference  
548 pressure, and thermobaricity, *J. Phys. Oceanogr.*, 33, 2504-2526. Doi:  
549 [http://dx.doi.org/10.1175/1520-0485\(2003\)033<2504:NASWTH>2.0.CO;2](http://dx.doi.org/10.1175/1520-0485(2003)033<2504:NASWTH>2.0.CO;2), 2003.

550 de Boyer Montegut, C., G. Madec, A. Fischer, A. Lazar, and D. Iudicone: Mixed Layer Depth  
551 over the Global Ocean: An Examination of Profile Data and a Profile-Based Climatology.  
552 *J. Geophys. Res.*, 109 (C12003), 1–20, doi:10.1029/2004JC002378, 2004.

553 D'Addezio, J. M., and Subrahmanyam, B.: Sea surface salinity variability in the Agulhas  
554 Current region inferred from SMOS and Aquarius. *Remote Sensing of Environment*, 180,  
555 440–452. doi:10.1016/j.rse.2016.02.006, 2016

556 Drange, H. and Simonsen, K.: Formulation of air-sea fluxes in the ESOP2 version of MICOM,  
557 Technical Report No. 125 of Nansen Environmental and Remote Sensing Center, 1996.

558 Droghei, R., Buongiorno Nardelli, B., and Santoleri, R.: A new global sea surface salinity and  
559 density dataset from multivariate observations (1993–2016). *Front. Mar. Sci.* 5:84. doi:  
560 10.3389/fmars.2018.00084, 2018

561 ESA, SMOS data products, available from  
562 <https://earth.esa.int/documents/10174/1854456/SMOS-Data-Products-Brochure> (last  
563 access on 12<sup>th</sup> December 2018), November 2017.

564 Font, J., Camps, A., Borges, A., Martín-Neira, M., Boutin, J., Reul, N., Kerr, Y. H., Hahne, A.,  
565 and Mecklenburg, S.: SMOS: The challenging sea surface salinity measurement from  
566 space, *Proc. IEEE*, 98(5), 649–665, DOI: [10.1109/JPROC.2009.2033096](https://doi.org/10.1109/JPROC.2009.2033096), May 2010.

567 Furue, R., Takatama, K., Sasaki, H., Schneider, N., Nonaka, M., and Taguchi, B.: Impacts of  
568 sea-surface salinity in an eddy-resolving semi-global OGCM. *Ocean Modelling*, 122, 36–  
569 56, doi:10.1016/j.ocemod.2017.11.004, 2018

570 Hátún, H., Sandø, A. B., Drange, H., Hansen, B., and Valdimarsson, H.: Influence of the  
571 Atlantic Subpolar Gyre on the Thermohaline Circulation, *Science*, 309 (5742), 1841-1844,  
572 doi:10.1126/science.1114777, 2005

573 Hunke, E. C., and Dukowicz, J. K.: An elastic-viscous-plastic model for sea ice dynamics, *J.*  
574 *Phys. Oceanogr.*, **27**, 1849-1867, [https://doi.org/10.1175/1520-](https://doi.org/10.1175/1520-0485(1997)027<1849:AEVPMF>2.0.CO;2)  
575 [0485\(1997\)027<1849:AEVPMF>2.0.CO;2](https://doi.org/10.1175/1520-0485(1997)027<1849:AEVPMF>2.0.CO;2), 1997.

576 Johnson, G. C., Schmidtko, S., and Lyman, J. M.: Relative contributions of temperature and  
577 salinity to seasonal mixed layer density changes and horizontal density gradients, *J.*  
578 *Geophys. Res.*, **117**, C04015, doi:[10.1029/2011JC007651](https://doi.org/10.1029/2011JC007651), 2012

579 Kerr, Y. H., Waldteufel, P., Wigneron, J. P., Delwart, S., Cabot, F., Boutin, J., Escorihuela, M.  
580 J., Font, J., Reul, N., Gruhier, C., Juglea, S., Drinkwater, M. R., Hahne, A., Martín-Neira,  
581 M., and Mecklenburg, S.: The SMOS mission: New tool for monitoring key elements of the  
582 global water cycle, *Proc. IEEE*, 98(5), 666–687, doi:[10.1109/JPROC.2010.2043032](https://doi.org/10.1109/JPROC.2010.2043032), 2010.

583 Kolodziejczyk, N., Boutin, J., Vergely, J.-L., Marchand, S., Martin, N., and Reverdin, G.:  
584 Mitigation of systematic errors in SMOS sea surface salinity. *Remote Sensing of*  
585 *Environment*, **180**, 164–177. doi:[10.1016/j.rse.2016.02.061](https://doi.org/10.1016/j.rse.2016.02.061), 2016

586 Latif, M., Roeckner, E., Mikolajewicz, U., and Voss R.: Tropical stabilization of the thermohaline  
587 circulation in a greenhouse warming simulation, *J. Clim.*, **13**: 1809–1813, 2000.

588 Macdonald, R. W., Carmack, E. C., McLaughlin, F. A., Falkner, K. K., and Swift, J. H.:  
589 Connections among ice, runoff and atmospheric forcing in the Beaufort Gyre. *Geophys.*  
590 *Res. Lett.*, **26**, 2223–2226, 1999

591 Maes, C., Ando, K., Delcroix, T., Kessler, W. S., McPhaden, M. J., and Roemmich,  
592 D.: Observed correlation of surface salinity, temperature and barrier layer at the eastern  
593 edge of the western Pacific warm pool, *Geophys. Res. Lett.*, **33**, L06601,  
594 doi:[10.1029/2005GL024772](https://doi.org/10.1029/2005GL024772), 2006.

595 Mathis, J. T., and Monacci, N. M.: Carbon Dioxide and Hydrographic data obtained during the  
596 USCGC Healy Cruise HLY1203 in the Arctic Ocean (October 05 - 25, 2012). Available  
597 from <http://cdiac.ess-dive.lbl.gov/ftp/oceans/CARINA/Healy/HLY-12-03/>. Oak Ridge  
598 National Laboratory, US Department of Energy, Oak Ridge, Tennessee. doi:  
599 [10.3334/CDIAC/OTG.CLIVAR\\_33HQ20121005](https://doi.org/10.3334/CDIAC/OTG.CLIVAR_33HQ20121005), 2014.

600 McPhee, M. G., Stanton, T. P., Morison, J. H. and Martinson, D. G.: Freshening of the upper  
601 ocean in the Arctic: is perennial sea ice disappearing? *Geophys. Res. Lett.* **25**, 1729–1732,  
602 1998.

603 Mecklenburg, S., Drusch, M., Kerr, Y. H., Font, J., Martín-Neira, M., Delwart, S., Buenadicha,  
604 G., Reul, N., Daganzo-Eusebio, E., Oliva, R., and Crapolicchio, R.: ESA's soil moisture  
605 and ocean salinity mission: Mission performance and operations. *IEEE TGARS*, **50**(5),  
606 1354–1366, DOI: [10.1109/TGRS.2012.2187666](https://doi.org/10.1109/TGRS.2012.2187666), 2012

607 Mignot, J., and Frankignoul, C.: On the interannual variability of surface salinity in the Atlantic.  
608 *Climate Dynamics*, **20**(6), 555–565. doi:[10.1007/s00382-002-0294-0](https://doi.org/10.1007/s00382-002-0294-0), 2003

609 Morison, J., Kwok, R., Peralta-Ferriz, C., Alkire, M., Rigor, I., Andersen, R., and Steele, M.:  
610 Changing arctic ocean freshwater pathways. *Nature*, 481:66–70, 2012.

611 Olmedo, E., Gabarró, C., González-Gambau, V., Martínez, J., Ballabrera-Poy, J., Turiel, A.,  
612 Portabella, M., Fournier, S., and Lee, T.: Seven Years of SMOS Sea Surface Salinity at  
613 High Latitudes: Variability in Arctic and Sub-Arctic Regions. *Remote Sensing*. 2018;  
614 10(11):1772, <https://doi.org/10.3390/rs10111772>, 2018.

615 Reverdin, G., Cayan, D., and Kushnir, Y.: Decadal variability of hydrography in the upper  
616 northern North Atlantic in 1948–1990. *J. Geophys. Res.*, 102, 8505–8531,  
617 <https://doi.org/10.1029/96JC03943>, 1997

618 Sakov, P., and Oke, P. R.: A deterministic formulation of the ensemble Kalman Filter: an  
619 alternative to ensemble square root filters. *Tellus A*, 60(2), 361-371, doi:10.1111/j.1600-  
620 0870.2007.00299.x, 2008.

621 Simmons, A., Uppala, S., Dee, D., and Kobayashi, S.: ERA-Interim: New ECMWF reanalysis  
622 products from 1989 onwards. *ECMWF Newsletter*. 110. 25-35, doi:10.21957/pocnex23c6,  
623 2007.

624 SMOS Team, SMOS L2 OS Algorithm Theoretical Baseline Document, ESA, Paris, France,  
625 SO-TN-ARG-GS-0007, version 3.13, available from  
626 [https://earth.esa.int/documents/10174/1854519/SMOS\\_L2OS-ATBD](https://earth.esa.int/documents/10174/1854519/SMOS_L2OS-ATBD) (last access: 12<sup>th</sup>  
627 December 2018), 29<sup>th</sup> April 2016.

628 SMOS-BEC Team, Quality Report: Validation of SMOS-BEC experimental sea surface salinity  
629 products in the Arctic Ocean and high latitudes Oceans. Years 2011-2013, Barcelona  
630 Expert Centre, Spain. Technical note: BEC-SMOS-0007-QR version 1.0, available at  
631 <http://bec.icm.csic.es/doc/BEC-SMOS-0007-QR.pdf> (last access: 13<sup>th</sup> December 2018),  
632 4<sup>th</sup> March 2016.

633 Steele, M. and W. Ermold (2004) Salinity Trends on the East Siberian Shelves, *Geophysical*  
634 *Research Letters*, Vol. 31, L24308, doi:10.1029/2004GL021302, 2004.

635 Steele, M., R. Morley, and W. Ermold, PHC: A global ocean hydrography with a high-quality  
636 Arctic Ocean, *Journal of Climate*, 14, 2079-2087, 2001.

637 Sumner, D., and Belaineh, G.: Evaporation, Precipitation, and Associated Salinity Changes at  
638 a Humid, Subtropical Estuary. *Estuaries*, 28(6), 844-855. Retrieved from  
639 <http://www.jstor.org/stable/3526951>, 2005.

640 Supply A, Boutin J, Vergely J-L, et al.: Precipitation Estimates from SMOS Sea-Surface  
641 Salinity. *Q. J. R. Meteorol. Soc.*, 144 (Suppl. 1):103–119, <https://doi.org/10.1002/qj.3110>,  
642 2018.

643 Talley, L. D., Johnson, G. C., Purkey, S., Feely, R. A., and Wanninkhof, R.: Global Ocean  
644 Ship-based Hydrographic Investigations Program (GO-SHIP) provides key climate-  
645 relevant deep ocean observations, *US CLIVAR Variations*, 15 (2), available from

646 <https://www.pmel.noaa.gov/pubs/PDF/tall4659/tall4659.pdf> (last access: 19th December  
647 2018), 2017.

648 Toole, J. M., Krishfield, R. A., Timmermans, M.-L., and Proshutinsky, A.: The Ice-Tethered  
649 Profiler: Argo of the Arctic, *Oceanography*, 24, 126–135, doi:10.5670/oceanog.2011.64,  
650 2011.

651 Tseng, Y., Bryan, F. O., and Whitney, M. M.: Impacts of the representation of riverine  
652 freshwater input in the community earth system model. *Ocean Modelling*, 105, 71–86.  
653 doi:10.1016/j.ocemod.2016.08.002, 2016.

654 Uotila, P., Goosse, H., Haines, K., Chevallier, M., Barthélemy, A., Bricaud, C., Carton, J.,  
655 Fuřkar, N., Garric, G., Iovino, D., Kauker, F., Korhonen, M., Lien, V. S., Marnela, M.,  
656 Massonnet, F., Mignac, D., Peterson, A., Sadikn, R., Shi, L., Tietsche, S., Toyoda, T., Xie,  
657 J., and Zhang, Z.: An assessment of ten ocean reanalyses in the polar regions, *Clim.*  
658 *Dynam.*, <https://doi.org/10.1007/s00382-018-4242-z>, online first, 2018.

659 Vancoppenolle, M., Fichefet, T., and Goosse, H.: Simulating the mass balance and salinity of  
660 Arctic and Antarctic sea ice. 2. Importance of sea ice salinity variations. *Ocean Modelling*,  
661 27, 54–69. doi:10.1016/j.ocemod.2008.11.003, 2009.

662 Verbrugge, N., Mulet, S., Guinehut, S., Buongiorno Nardelli, B., and Droghei, R.: Quality  
663 information document for global ocean multi observation products  
664 multiobs\_glo\_phy\_rep\_015\_002, CMEMS-MOB-QUID-015-002, v1.0, available from  
665 <http://cmems-resources.cls.fr/documents/QUID/CMEMS-MOB-QUID-015-002.pdf> (last  
666 access: 14<sup>th</sup> December 2018), February 2018.

667 Vialard, J., and P. Delecluse (1998), An OGCM study for the TOGA decade: I. Role of salinity  
668 in the physics of the Western Pacific fresh pool, *J. Phys. Oceanogr.*, 28, 1071–1088.

669 Woodgate, R., Aagaard, K. and Weingartner, T.: Monthly temperature, salinity, and  
670 transport variability of the Bering Strait through flow. *Geophys. Res. Lett.*, 32, L04601,  
671 DOI: 10.1029/2004GL021880, 2005.

672 Xie, J., Bertino, L., Counillon, F., Lisæter, K. A., and Sakov, P.: Quality assessment of the  
673 TOPAZ4 reanalysis in the Arctic over the period 1991–2013. *Ocean Science*, 13(1), 123–  
674 144. <http://doi.org/10.5194/os-13-123-2017>, 2017.

675 Xie, J., Counillon, F., and Bertino, L.: Impact of assimilating a merged sea-ice thickness from  
676 CryoSat-2 and SMOS in the Arctic reanalysis, *The Cryosphere*, 12, 3671-3691,  
677 <https://doi.org/10.5194/tc-12-3671-2018>, 2018.

678 Xie, J., Counillon, F., Bertino, L., Tian-Kunze, X., and Kaleschke, L.: Benefits of assimilating  
679 thin sea-ice thickness from SMOS into the TOPAZ system. *The Cryosphere*, 10, 2745–  
680 2761. <http://doi.org/10.5194/tc-10-2745-2016>, 2016.

681 Yu, L.: A global relationship between the ocean water cycle and near-surface salinity, J.  
682 Geophys. Res., 116, C10025, doi:10.1029/2010JC006937, 2011.  
683 Zweng, M. M., Reagan, J. R., Antonov J. I., Locarnini, R. A., Mishonov, A. V., Boyer, T. P.,  
684 Garcia, H. E., Baranova, O. K., Johnson, D. R., Seidov, D., and Biddle, M. M.: World  
685 Ocean Atlas 2013, Volume 2: Salinity, Levitus, S. (Ed.), Mishonov, A., Technical Ed.  
686 NOAA Atlas NESDIS 74, 39pp, 2013.  
687

### Captions of Table and Figures:

**Table 1.** Details of the six products evaluated during 2011-2013.

<i>Product</i>	<i>Data source</i>	<i>Resolution</i>	<i>Provider</i>	<i>Website or CMEMS id</i>	<i>Release year</i>
<b>BEC</b>	SMOS	9 days; 25 km	Barcelona Expert Centre, Spain	<a href="http://bec.icm.csie.es">http://bec.icm.csie.es</a>	2018
<b>CEC</b>	SMOS	9 days; 25 km zonal	Ocean Salinity Expertise Center, IFREMER	FTP: <a href="ftp.ifremer.fr">ftp.ifremer.fr</a>	2018
<b>TP4</b>	Reanalysis	Daily; 12~16 km	CMEMS	ARCTIC-REANALYSIS-PHYS-002-003	2015
<b>MOB</b>	In situ + SMOS	7 days; 1/4x1/4°;	CMEMS	MULTIOBS_GLO_PHY_REP_015_002	2016
<b>PHC</b>	In situ (1950-1994)	Monthly; 1x1°	<i>Polar Science Center, University of Washington</i>	<a href="http://psc.apl.washington.edu/">http://psc.apl.washington.edu/</a>	2005
<b>WOA</b>	In situ (1955~2012)	Monthly; 1/4x1/4°	NODC, NOAA	<a href="https://www.nodc.noaa.gov/O_C5/woa13/">https://www.nodc.noaa.gov/O_C5/woa13/</a>	2013

**Table 2.** Misfits of SSS relative to in-situ CORA5.1 observations during 2011-2013 in each sub-region. Bold numbers denote the smallest error among the six products.

Region	Bias (psu)						RMSD (psu)					
	BEC	CEC	TP4	MOB	PHC	WOA	BEC	CEC	TP4	MOB	PHC	WOA
S0	-	-	.48	-.52	.48	<b>-.11</b>	-	-	1.25	1.78	1.28	<b>.70</b>
S1	4.03	3.18	3.29	1.63	3.29	<b>.42</b>	4.23	3.70	3.47	2.22	3.43	<b>1.37</b>
S2	-1.76	<b>-.44</b>	-.97	2.96	-3.30	-2.93	2.16	2.57	<b>1.70</b>	3.68	3.87	3.62
S3	<b>-.14</b>	-.70	<b>-.14</b>	-.21	-.29	-.25	.45	1.17	<b>.34</b>	.42	.51	.44
S4	-.09	-.20	.12	.11	<b>-.02</b>	<b>.02</b>	.91	1.21	.89	.86	.94	<b>.84</b>
S5	-.07	.06	.20	<b>.01</b>	.02	.07	1.47	1.52	1.42	1.44	1.39	<b>1.30</b>
S6	<b>-.01</b>	.15	<b>.01</b>	<b>-.01</b>	-.09	.05	.25	.66	.14	<b>.12</b>	.28	.16
S7	.05	.34	.04	<b>-.03</b>	-.23	<b>-.03</b>	.31	.88	.33	<b>.22</b>	.43	.27

**Table 3.** Optimal coefficients for the 4<sup>th</sup> order polynomial fit of the errors (see Eq. 3) as a function of in-situ SSS for each product.

Product	F(p <sub>1</sub> , p <sub>2</sub> , p <sub>3</sub> , p <sub>4</sub> , p <sub>5</sub> , S)					Residual norm	In situ samples
	p <sub>1</sub> (x10 <sup>-3</sup> )	p <sub>2</sub>	p <sub>3</sub>	p <sub>4</sub>	p <sub>5</sub>		
BEC	0.168	-0.016	0.614	-11.345	87.097	7.03	91
CEC	0.225	-0.033	-1.550	-29.886	205.179	18.13	121
TP4	0.993	-0.096	3.430	-54.552	335.197	10.17	232
MOB	-1.080	0.128	-5.469	99.824	-645.087	68.81	163
PHC	1.257	-0.120	4.235	-65.938	388.808	13.98	232
WOA	-0.121	0.010	-0.322	3.998	-10.847	38.91	232

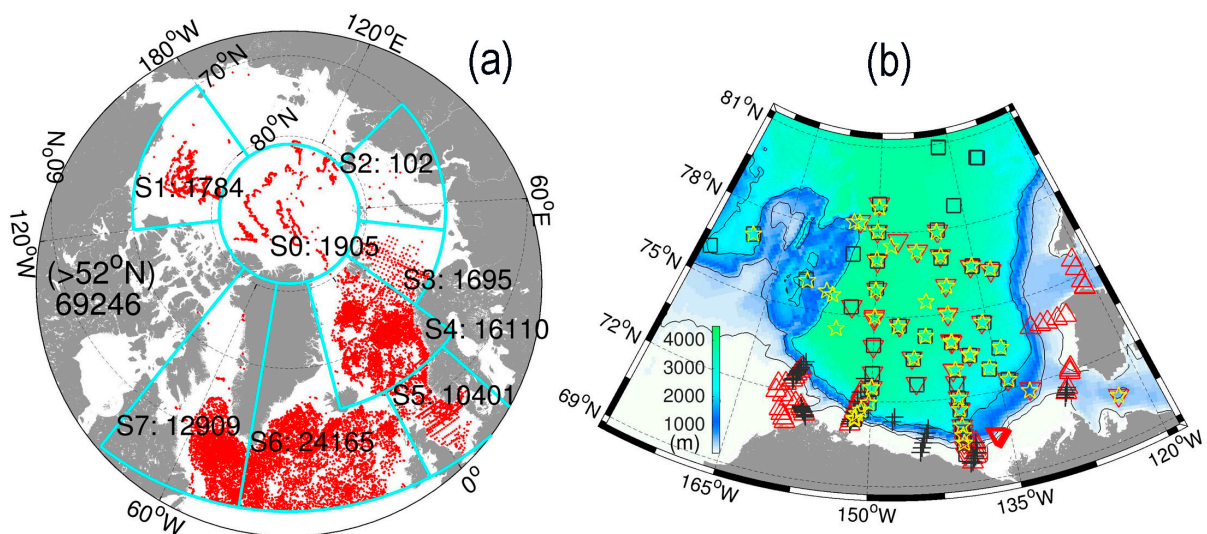


**Fig. 1** (a): SSS locations of the in-situ observations north of 52°N in CORA5.1 during the years 2011-2013. 8 sub-regions divide the Arctic Ocean, with the number of observations indicated in each region. (b): Independent SSS observations in the Beaufort Sea during the summer months of 2011-2013 from the BGP (marked by anti-triangles, squares, and stars) and the CLIVAR (marked by triangles and crosses). Different colors (red, black and yellow) indicate the years (2011, 2012 and 2013 resp.).

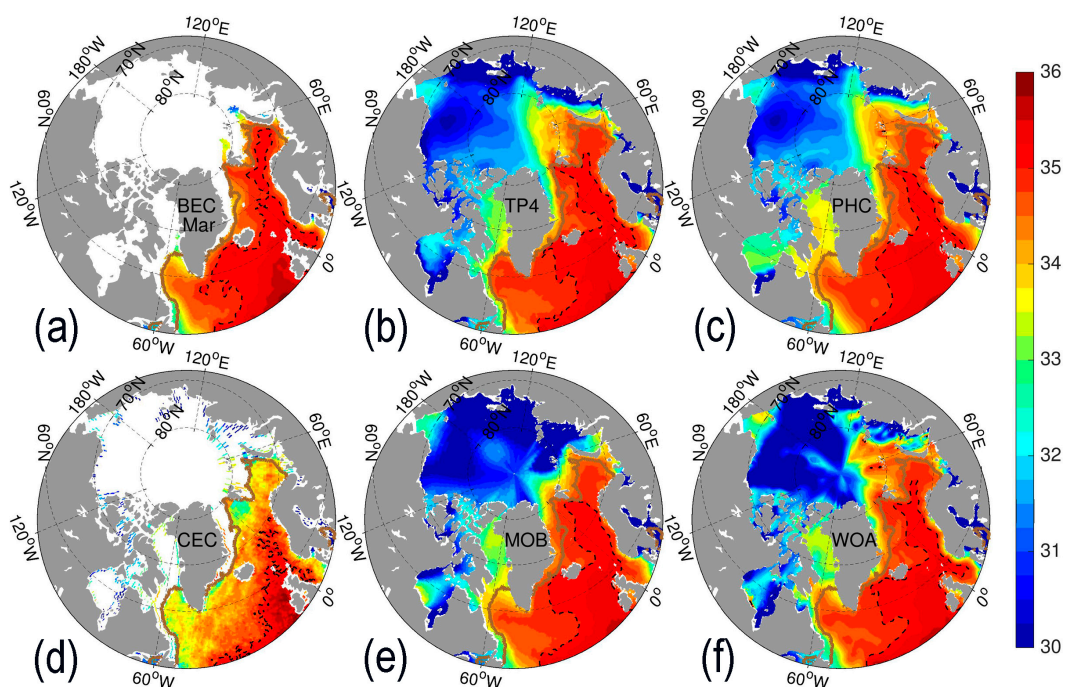


**Fig. 2** Monthly SSS (unit: psu) in March from satellite products (BEC and CEC, *left column*), reanalysis/reprocessing (TP4 and MOB, *middle column*), and climatology (PHC and WOA, *right column*). White areas are masked by sea ice. The thick brown line represents the sea ice edge (15% concentration from TP4), and the black shaded isoline represents the 35 psu salinity near the surface.

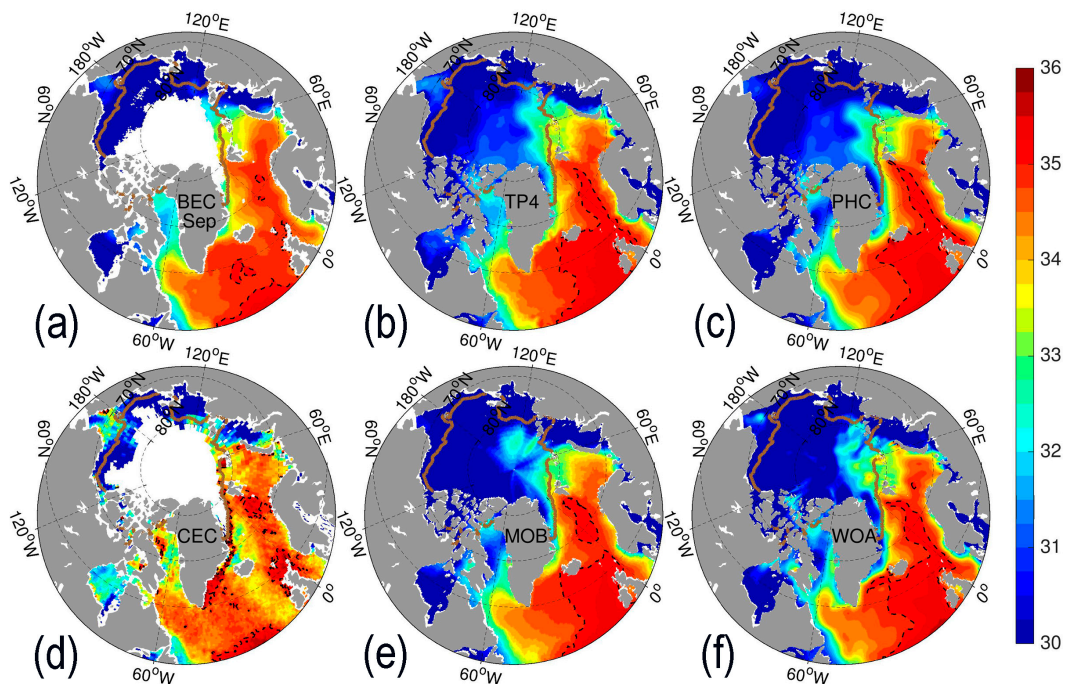


Fig. 3 Similar to previous figure in September.

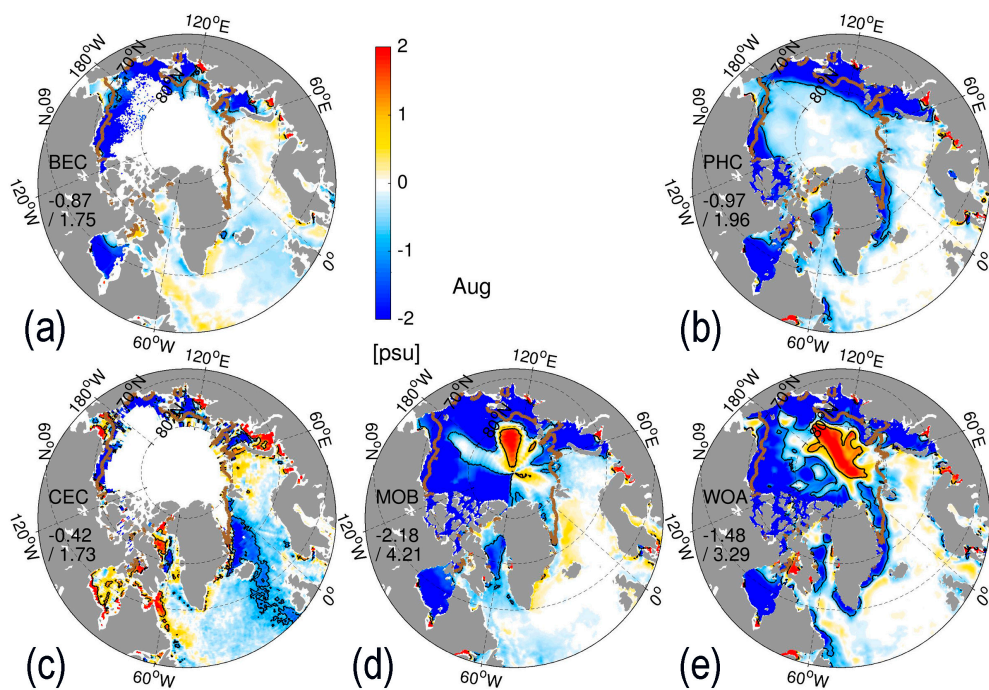


Fig. 4 Deviations of monthly SSS (unit: psu) in August for (a) BEC; (b) PHC; (c) CEC; (d) MOB; and (e) WOA relative to TP4. The thick brown line represents sea ice edge (15% concentration from TP4), the black lines represent  $\pm 1$  psu.

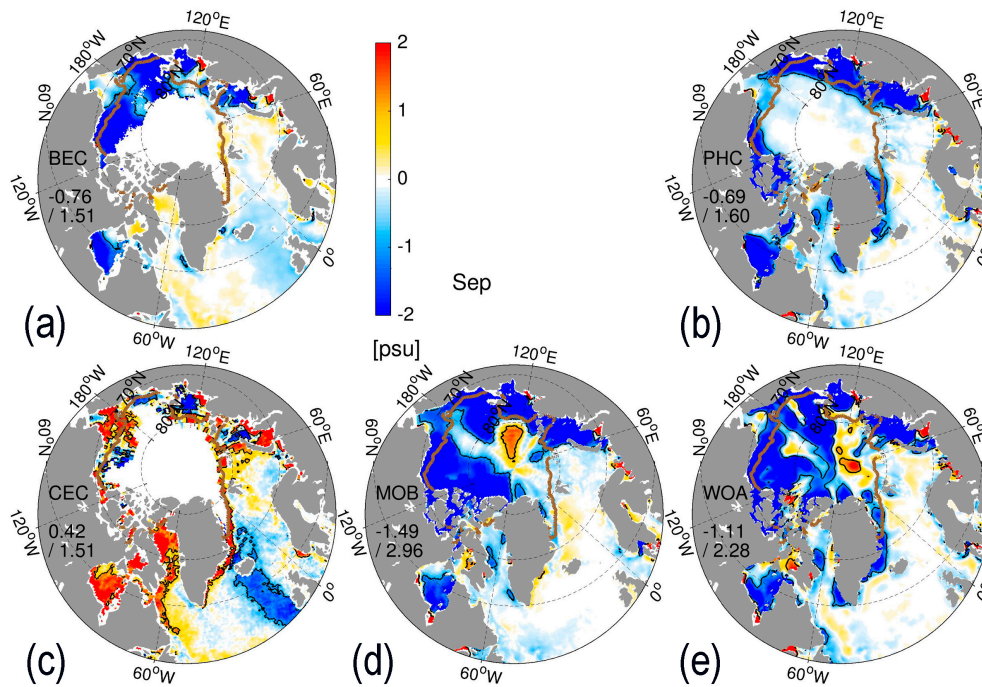


Fig. 5 Same as previous for September.

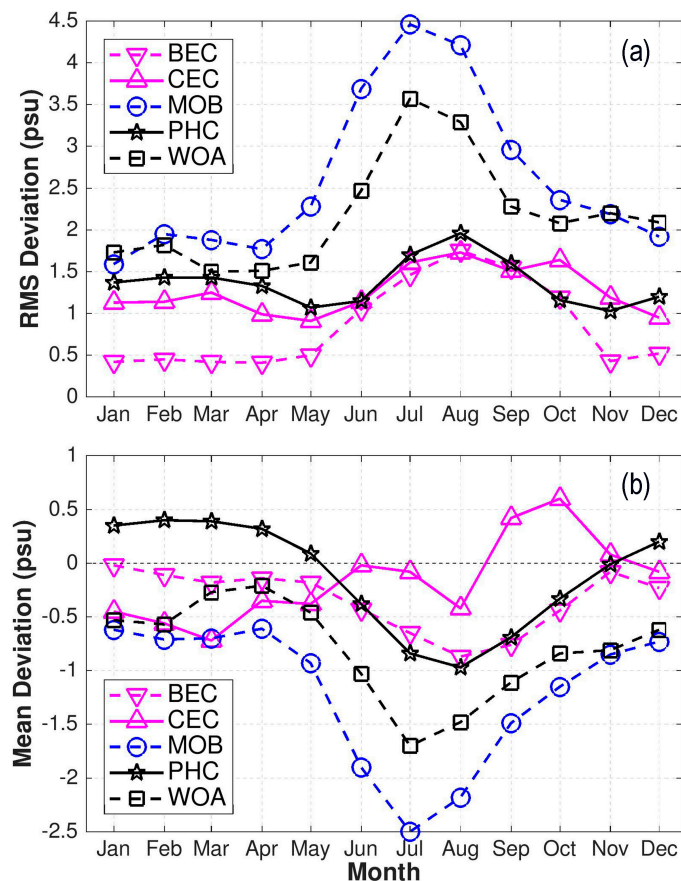
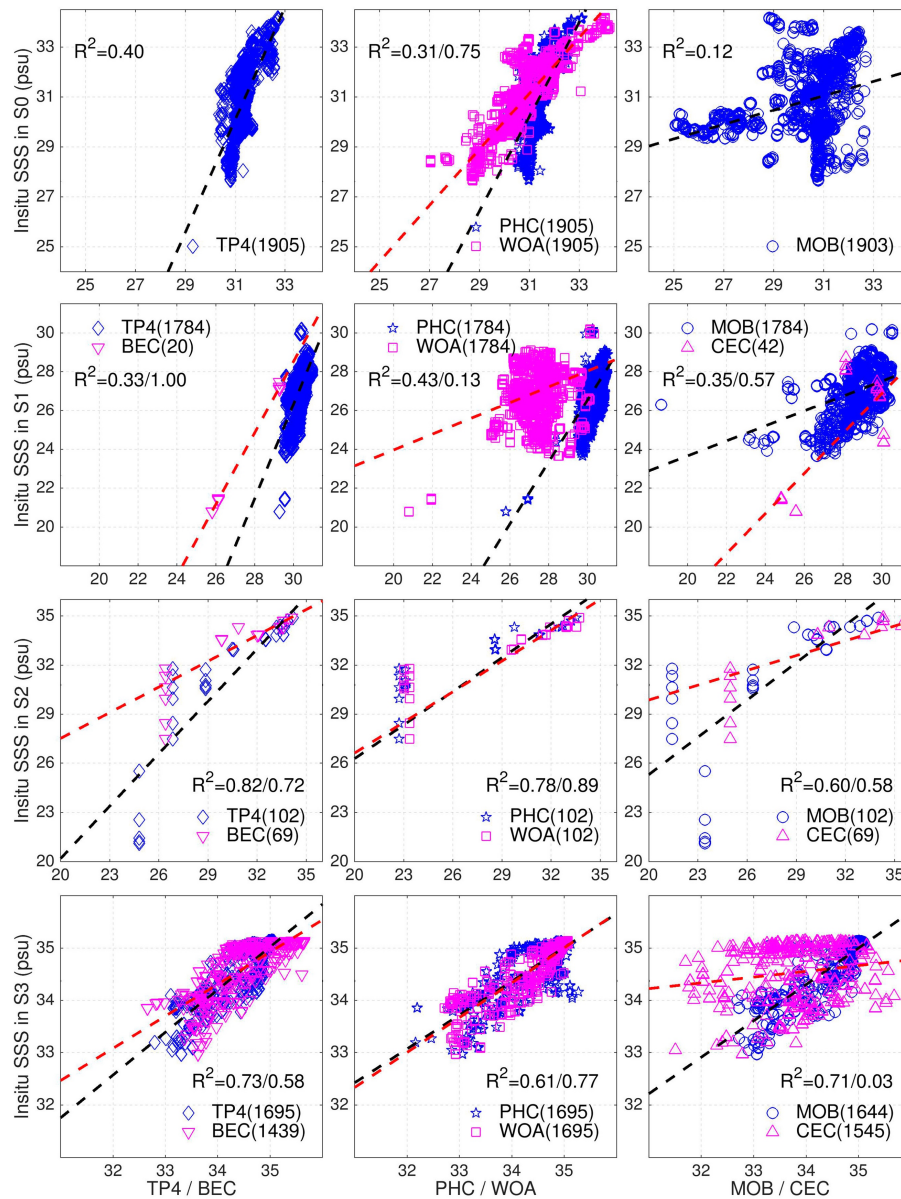


Fig. 6 Monthly deviations in the Arctic Ocean (>60N) of (a) the RMS and (b) the spatial average during the period 2011-2013 for the five SSS products referred to TP4. The anti-triangle (triangle, circle, star and square) line represents the SSS deviations from BEC (CEC, MOB, PHC and WOA respectively).



**Fig. 7** Scatterplots of SSS compared to the CORA5.1 in-situ observations with respect to the S0-S3 regions in the Arctic. The diamonds (anti-triangles, stars, squares, circles, and triangles) represents the SSS from TP4 (BEC, PHC, WOA, MOB, and CEC respectively). The black (red) lines are the linear regressions of the blue (purple) dots in each panel, and the coefficient  $R^2$  is indicated in the panel together with the number of observations in parentheses.

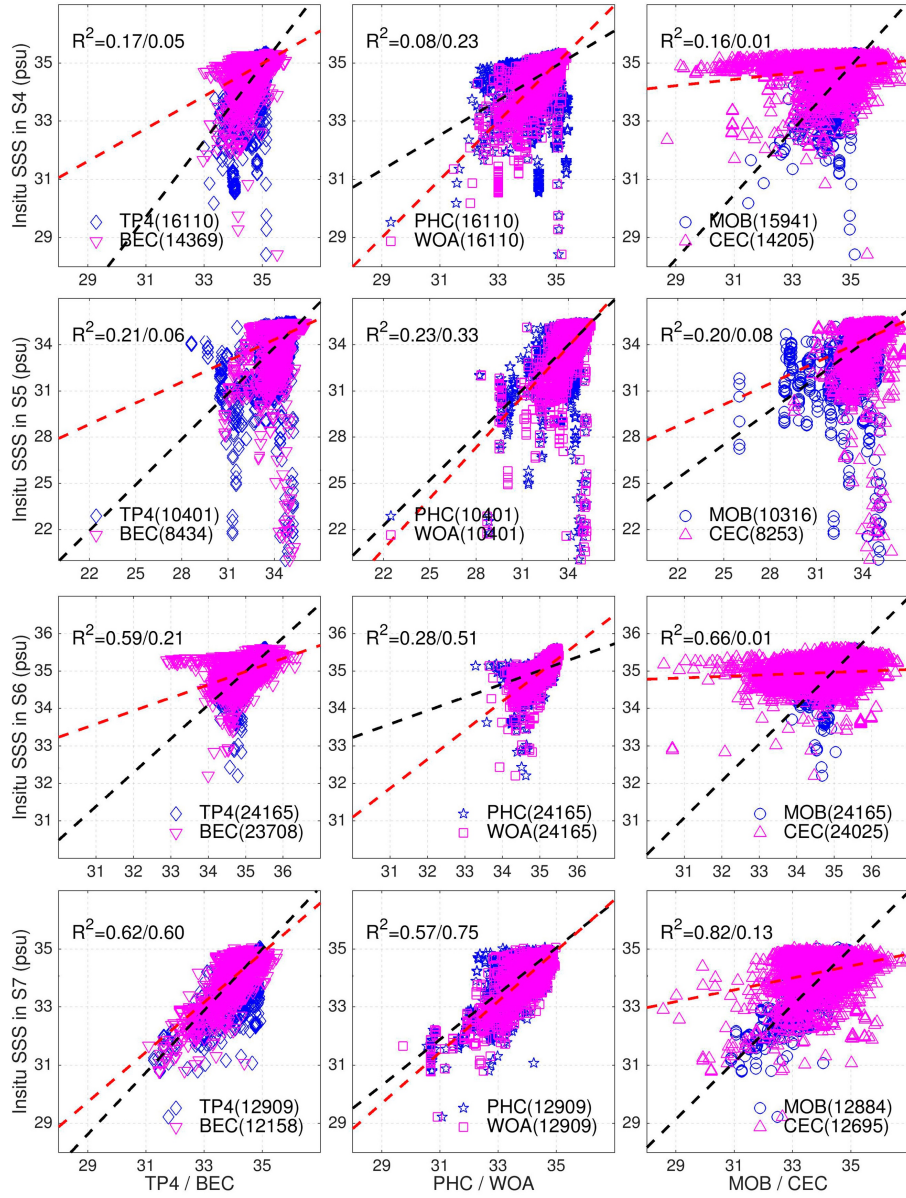
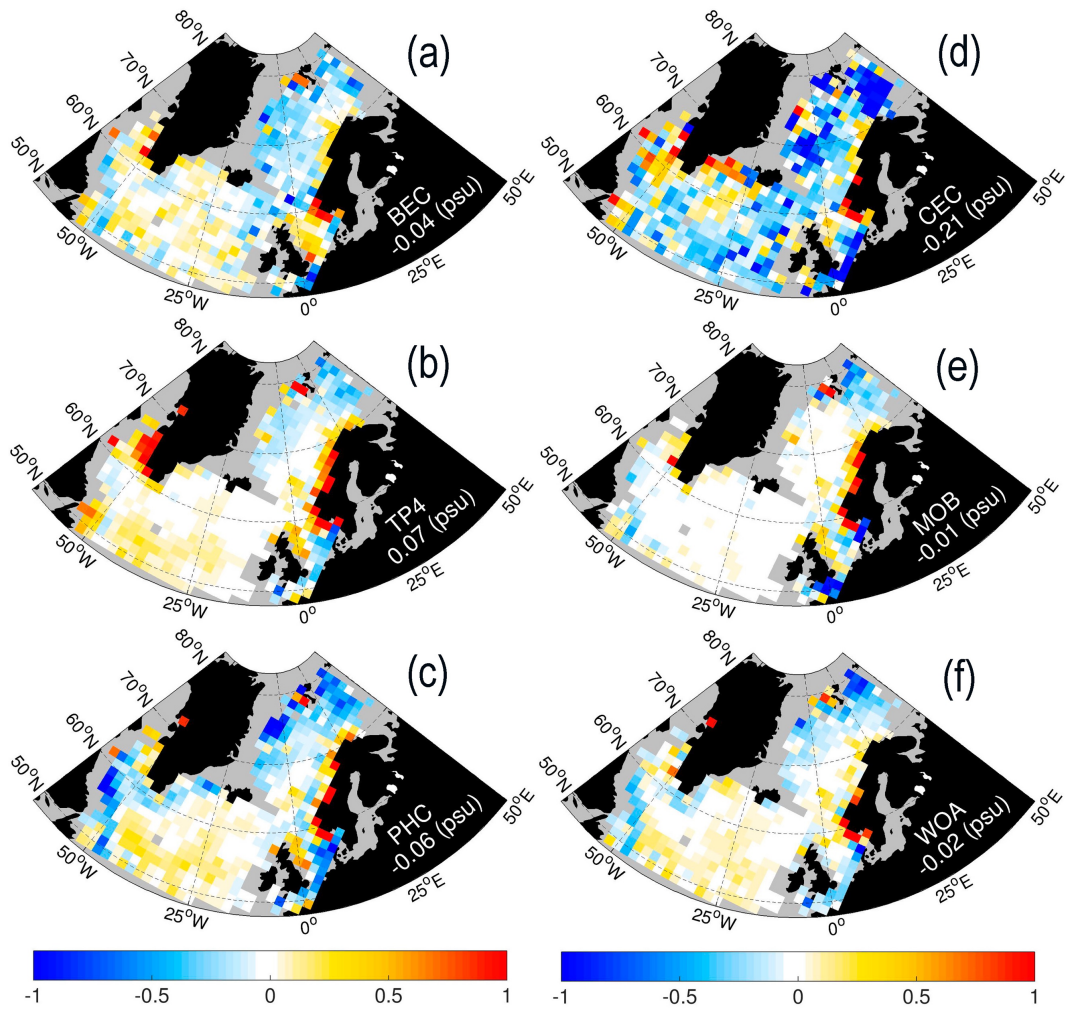
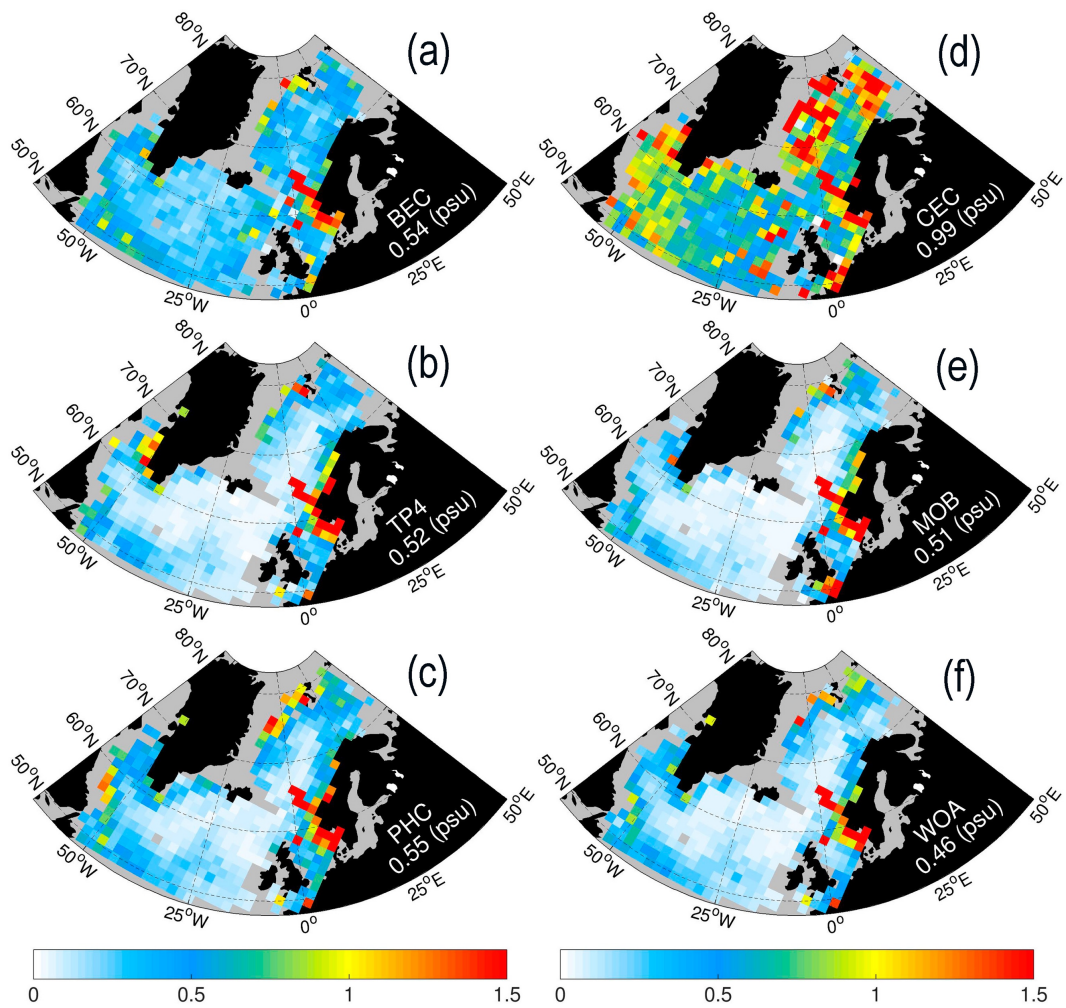


Fig. 8 Same as Fig. 7 but for the subpolar regions S4-S7.



**Fig. 9** The mean deviation of SSS for the six datasets compared to in situ observations from CORA 5.1 during the three years of 2011-2013 in the northern North Atlantic and the Nordic seas. The SSS observations are distributed into the coarse grid cells of 9x9 grids in TP4, with a gray mask if the valid observations less than 10.



**Fig. 10** The Root Mean Square deviation of SSS for six datasets compared to in situ observations from CORA 5.1 during the three years of 2011-2013 in the northern North Atlantic and the Nordic seas. The SSS observations are distributed into the coarse grid cells of 9x9 grids in TP4, with a grey mask if the valid observations less than 10.

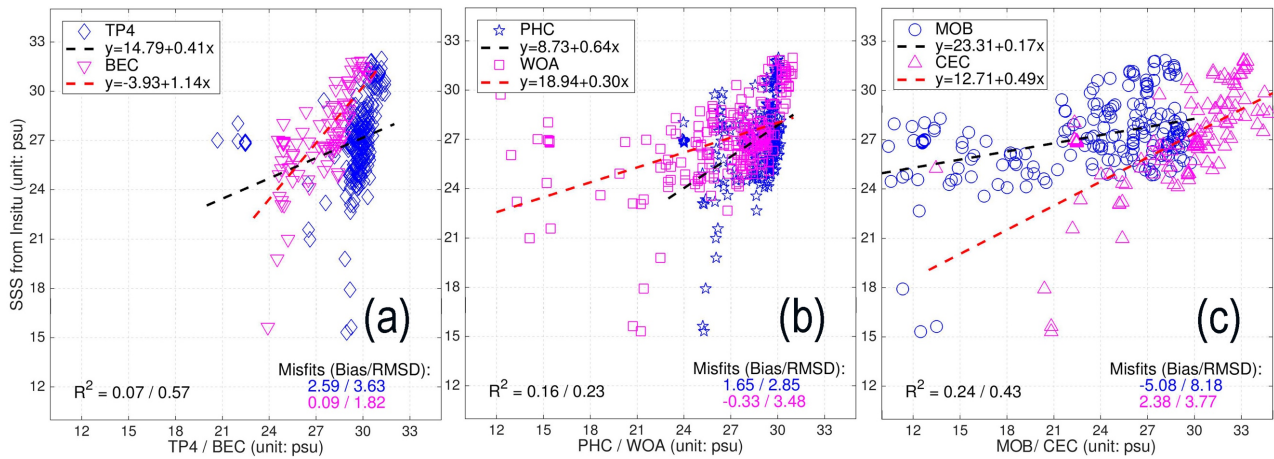


**Fig. 11** Scatterplots of SSS compared to the in-situ observations in Beaufort Sea during the summer months of 2011-2013: (a) The diamond (anti-triangle) represents the SSS from TP4 (BEC) with blue (purple), and the linear regression is denoted by the dashed black (red) line. (b) The star (square) from the climatology of PHC (WOA). (c) The circle (triangle) represents from MOB (CEC). The coefficient  $R^2$  is the squared linear relationship, and the misfits also shown on the panels.

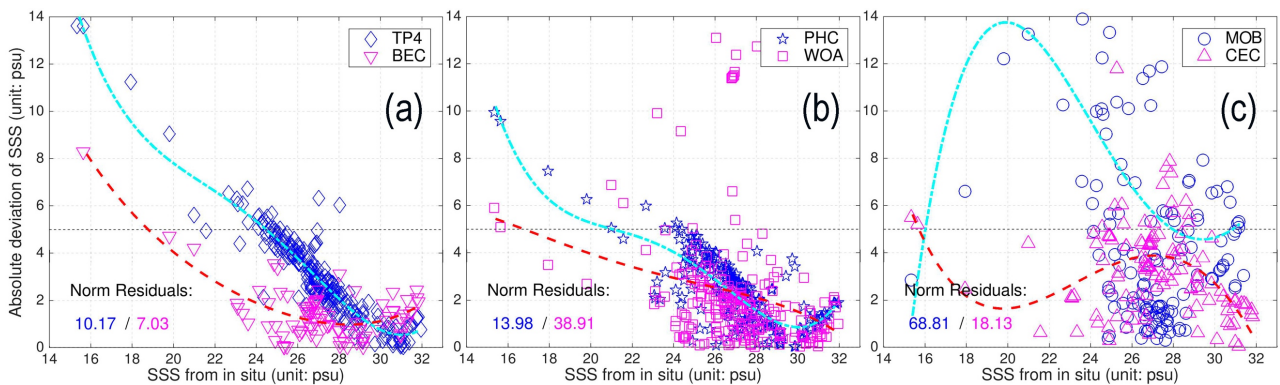


**Fig. 12** Scatterplots of SSS uncertainty compared to the in-situ observations in Beaufort Sea as a function of the observed salinity. The black dashed line represents the absolute deviation of 5 psu. (a) The diamond (anti-triangle) represents from TP4 (BEC) with blue (purple). (b) The star (square) from the climatology of PHC (WOA). (c) The circle (triangle) represents from MOB (CEC). The thick dashed curves are fitted by the fourth order polynomial function, and the norm residuals are marked on panel respectively.